Journal of GeoEngineering, Vol. 17, No. 4, pp. 195-206, December 2022
http://dx.doi.org/10.6310/jog.202212_17(4).3

IMPEDANCE EFFECT OF BAFFLE PILES ON GRANULAR FLOW: A NUMERICAL INVESTIGATION USING COUPLED EULERIAN-LAGRANGIAN TECHNIQUE

Chih-Hsuan Liu [1], Kevin Suryo [2], Ching Hung [3*]

ABSTRACT

A validated Coupled Eulerian-Lagrangian technique was used to study the impedance effect of baffle piles on granular behavior. This study focuses on the impact force acting on the rigid barrier and the baffle piles, the arrival time of the granular flow to the rigid barrier, and the variation of kinetic energy during the flow. The position of the baffle piles along the slope, the angle of the slope, and the shape of the baffle piles were considered in the study. Based on the results, it was found that the baffle piles can significantly reduce the impact force acting on the rigid barrier and delay the arrival time of the granular flow to the rigid barrier. It is also shown that the impedance effect of baffle piles increases with increasing the angle of the slope; however, on steep slopes, the baffle pile should be carefully considered so that the granular material does not fly and hit the rigid barrier directly. Finally, circular baffle piles have been shown to absorb less impact force.

Key words: Coupled Eulerian-Lagrangian technique, granular flow, baffle piles, impact force, impedance effect.

1. INTRODUCTION

Granular flows, such as debris flows and rock avalanches, are among the most devastating geohazards and can pose a significant threat to infrastructure, assets, and life. To reduce the risk posed by granular flows, it is important to design effective structural mitigation measures such as check dams (Jeong and Lee 2019; Lee *et al*. 2019), flexible barriers (Kwan *et al*. 2019; Siyou *et al*. 2020), curved barriers (Choi *et al.* 2017), and baffle piles (Li *et al.* 2020). Check dams, flexible barriers, and curved barriers are generally classified as catching structures, and baffle piles are classified as retarding structures. In general, these structural mitigation measures dissipate the kinetic energy of the granular flow and change the direction of the flow.

The catching structure is an effective means of retaining granular flows and resisting impacts along the flow path. However, this type of structure is expensive for large applications, and high-speed, large-scale granular flows can overcome the catching structure (Jianbo *et al*. 2020; Li *et al*. 2020). In contrast, retarding structures, in particular arrays of baffle piles, are effective in dissipating the kinetic energy of granular flow and are rather adaptive. As a result, arrays of baffle piles have recently become a more widely used structural mitigation measure (Bi *et al*. 2018; Li *et al*. 2020).

A practical design for an array of baffle piles relies on the impact force evaluation of granular flow. Consequently, researchers have developed small- to full-scale experimental tests (Ng *et al*. 2012; Ng *et al*. 2014; Jianbo *et al*. 2020) and conducted numerical analyses (Mast et *al*. 2014; Choi and Law 2015; Bi *et al*. 2018, 2019; Li *et al*. 2020) to thoroughly study the impact mechanism, the layout of baffle piles, and the kinetic behaviors of granular flow. For example, Jianbo *et al*. (2020) conducted small-scale laboratory experiments on granular flow, identifying the impedance effects of the distance between the baffle piles and the foot of the slopes. Li *et al*. (2020) investigated the influence of baffle piles on the debris flow of real landslides and found that the geometry and arrangement of baffle piles had significant effects on the movement and deposition of debris. Using the flume tests and numerical discrete element analyses (DEA), Choi and Law (2015) studied the optimal configuration of the baffle arrays for landslide debris. Bi *et al*. (2018) conducted a series of DEA to investigate the effect of a combined baffle avalanche wall system on the kinetic impedance of rock avalanches.

The main issues from the previous research so far include: 1. The maximum impact force generally increases with steeper slopes (Moriguchi *et al*. 2009; Lin *et al*. 2020); however, few studies have focused on the effect of slope angles. 2. Baffle piles installed upstream to reduce the impact acting on the barrier have not been well studied (Cosenza *et al*. 2006; Ng *et al*. 2015). 3. Most of the baffle piles were rectangular (Choi and Law 2014, 2015; Ng et *al*. 2014, 2015; Bi *et al*. 2019; Li *et al*. 2020); however, Shen *et al*. (2018), Wang *et al*. (2018), and Huang *et al*. (2021) show that the use of rectangular baffle piles may lead to poorer performance in terms of the destruction potential. Consequently, the above-mentioned issues can be addressed to enhance the effect of baffle piles.

Small- to full-scale experimental tests can reveal more realistic kinetic behaviors of granular flow via advanced experimental measurements (Crosta *et al*. 2009; Song *et al.* 2017; Lin *et al*. 2020; Luong *et al*. 2020). Nevertheless, the scale effect and sampling can complicate the acquisition of representative results using experimental tests. Advanced numerical and large deformation analysis techniques, such as the smoothed particle hydrodynamics

Manuscript received July 11, 2022; revised August 9, 2022; accepted September 4, 2022.
[1] Research Fellow, Ph.D., Department of Civil Engineering, National Cheng Kung University, Tainan, Taiwan.
[2] Master Student, Department of Civil Engineering, National Cheng Kung University, Tainan, Taiwan.
[3*] Associate Professor (corresponding author), Department of Civil Engineering, National Cheng Kung University, Tainan, Taiwan (e-mail: ChingHung@gs.ncku.edu.tw).

(SPH) method, the material-point-method (MPM), and the discrete element method (DEM), have been developed, and their capability in modeling the debris flows has been demonstrated (Chen and Qiu 2012; Mast *et al*. 2014; Choi and Law 2015; Bi *et al*. 2018; Neto and Borja 2018; Li *et al*. 2020; Nguyen *et al*. 2020; Nguyen *et al*. 2022). However, SPH and MPM techniques are not capable of reaching the accuracy achieved by finite element analysis (Chen and Lee 2004; Lee and Jeong 2018; Jeong and Lee 2019), and DEM would require calibrations of the micro-parameters given that these parameters may not be easily obtained from experimental studies (Coetzee 2017; Zhang *et al*. 2018). DEM may be more applicable to small-scale simulations due to the computation cost (Fei *et al*. 2020). Recently, the coupled Eulerian-Lagrangian (CEL) technique has been proved to be able to estimate the behavior of granular flow and fluid-solid interactions (Lee and Jeong 2018; Jeong and Lee 2019; Lee *et al*. 2019; Troncone *et al*. 2019; Lin *et al*. 2020). The use of the CEL technique does not require calibration of the micro-parameters of the material because the macro-parameters can be adopted.

In this study, a CEL technique is used to investigate the impedance effect of the impact force acting on the rigid barrier and baffle piles, the arrival time of the granular flow to the rigid barrier, and the variations in kinetic energy under various conditions were evaluated. The findings are expected to help improve the design of baffle piles.

2. CALCULATION PROCEDURE OF THE COUPLED EULERIAN-LAGRANGIAN (CEL) TECHNIQUE

The calculation procedure for the coupled Eulerian-Lagrangian technique was based on ABAQUS/Explicit (Hibbitt *et al*. 2019). Details pertaining to the calculation procedure of the CEL technique and the governing equation between the Lagrangian and Eulerian formulations can be found in the literature (Hibbitt *et al*. 2019; Hsu 2019; Lin *et al*. 2020). In this paper, only a brief introduction is presented.

For the calculation procedure, the mass, momentum, and energy conservation equation in Lagrangian form can be presented as:

$$\frac{d\rho}{dt} + \rho\nabla \cdot v = 0 \tag{1}$$

$$\rho\frac{dv}{dt} = \nabla \cdot \sigma + \rho b \tag{2}$$

$$\frac{de}{dt} = \sigma : D \tag{3}$$

where ρ is the material density, v is the material velocity, b is body force, e is the internal energy per unit volume, σ is the Cauchy stress, and D is the strain rate. In an Eulerian field $y(x, t)$, which is a tensor field with spatial coordinates x and time t, the total change rate of $y(x, t)$ is calculated based on the chain rule:

$$\frac{dy(x,t)}{dt} = \frac{\partial y(x,t)}{\partial t} + v \cdot [\nabla y(x,t)] \tag{4}$$

Equations (1)-(3), which are the employed Lagrangian formulations, can be converted to Eulerian formulation by applying Eq. (4).

$$\frac{\partial\rho}{\partial t} + \nabla \cdot (\rho v) = 0 \tag{5}$$

$$\frac{\partial\rho v}{\partial t} + \nabla \cdot (\rho v \otimes v) = \nabla \cdot \sigma + \rho b \tag{6}$$

$$\frac{\partial e}{\partial t} + \nabla \cdot (ev) = \sigma : D \tag{7}$$

Following Eqs. (5)-(7), the Eulerian formulation would lead to a general conservation form as follows:

$$\frac{\partial y}{\partial t} + \nabla \cdot \phi = S \tag{8}$$

where ϕ is the flux function and S is the source term.

The calculation procedure solves Eq. (8) by dividing it into Eqs. (9) and (10):

$$\frac{\partial y}{\partial t} = S \tag{9}$$

$$\frac{\partial y}{\partial t} + \nabla \cdot \phi = 0 \tag{10}$$

where Eqs. (9) and (10) are referred to as the Lagrangian and Eulerian steps, respectively.

The calculation procedure for the CEL technique is shown in Fig. 1. The mesh undergoing the deformation in the Lagrangian step is reshaped to the original regular mesh in the Eulerian step. A discrete field was created using the volume fraction tool based on the Eulerian part. The reference part with the Eulerian part can be determined as the volume ratio, which is based on the Eulerian volume fraction (EVF) of each element. Each element in the Eulerian part has a representative percentage of the region occupied by a specified material. Material-free and material-filled element areas are represented by 0 and 1, respectively. During each computation step of CEL analysis, the material and all the field variables are stored in the nodes and mapped onto the computational mesh (steps 1-2). The unknown field variables are then calculated by Lagrangian formulation, and the resulting acceleration, velocity, and displacement stored in each node are updated (step 3).

Additionally, strains and stresses are estimated by the constitutive model adopted in the analysis. The positions of the nodes are also updated after a mesh adjustment (step 4). The materials can flow freely in the spatially fixed discrete meshes without resistance until the element is filled with material. In the Eulerian step, the deformed mesh is remapped to the original regular mesh, and the material volume transportation between adjacent elements is calculated by the volume fraction tool (step 5). Finally, the energy, momentum, stress, and strain calculated in the Lagrangian step are adjusted accordingly to the material flow between adjacent elements (step 6).

Automatic time incrementation was adopted in this study to control the out-of-balance force at the node during the CEL calculation. The automatic time incrementation scheme provides a stability limit for the time increment of each computation step according to the current dilatational wave speed in each element and the highest element frequency in the whole model. All the faces of the box are fixed in all directions (X, Y, and Z directions), as shown in Fig. 2.

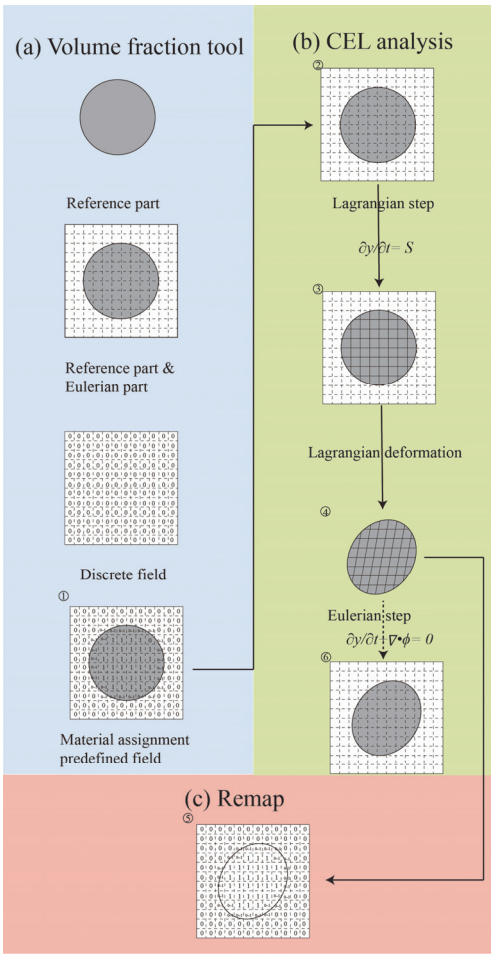

Fig. 1 The calculation proced of the CEL technique (after Lin *et al.* 2020)

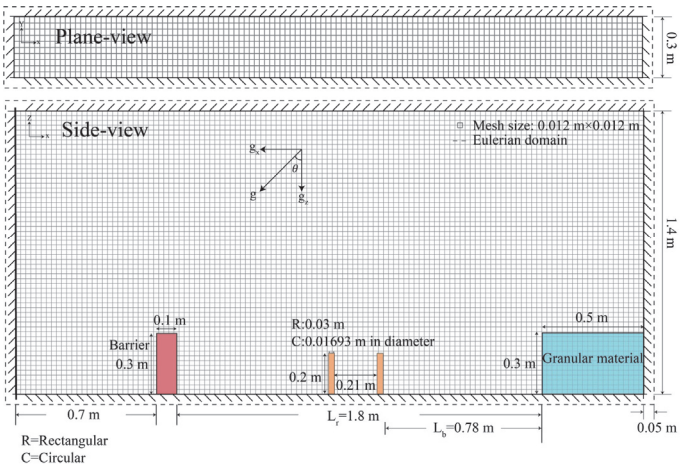

Fig. 2 Schematic of the CEL model

In this study, the default general contact model, based on the penalty contact algorithm, was applied to simulate the Eulerian-Lagrangian contact behaviors. The penalty contact algorithm automatically computes and tracks the interface between the Lagrangian structure and the Eulerian materials during the simulation. The contact force, F_p, between Eulerian and Lagrangian elements can be determined by the following equation:

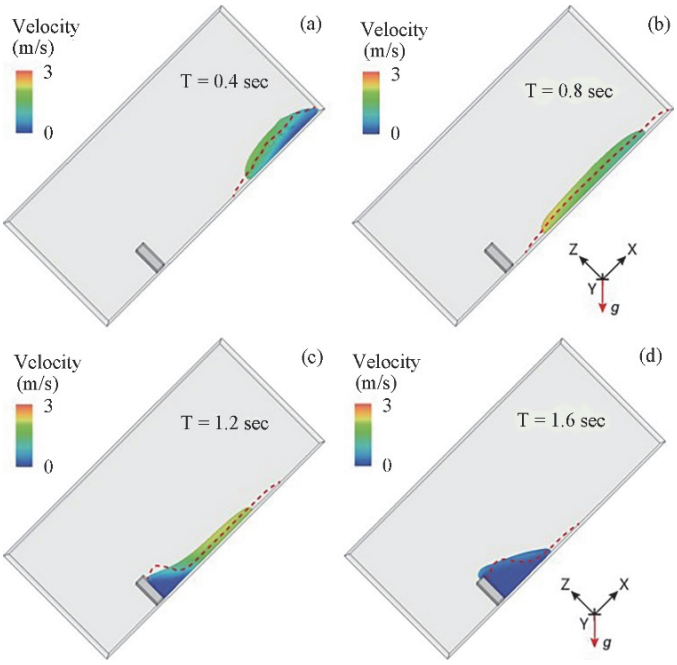

Fig. 3 Comparison of free surface configurations for the flowing sand between experimental results (red dot line) and CEL simulations (adopted from Lin *et al.* 2020)

$$F_p = k_p d_p \tag{11}$$

where k_p is the penalty stiffness, which depends on the material properties of the interactive elements and d_p is the penetration distance.

3. MODEL VALIDATION

CEL modeling was validated against data from small-scale laboratory tests (sandbox model) conducted by Moriguchi *et al.* (2009), which were widely adopted to validate the granular flow-structure interaction and consequent impact force (Crosta *et al.* 2009; Lee and Jeong 2018). The dimensions of the sandbox model were $1.4 \times 4 \times 0.2$ m (height, length, and width, respectively). The granular material with a length of 0.5 m, a height of 0.3 m, and a width of 0.2 and a barrier with a length of 0.7 m, a height of 3 m, and a width of 0.2 m were placed on the right side of the sandbox and 1.8 m in front of the granular material, respectively.

The Eulerian domain was fixed and larger than the sandbox model, with each dimension extended by 0.05 m. Only granular material was assigned to the Eulerian mesh to allow the granular media to flow through the Eulerian elements during the analysis. The granular material (flow mobility) was characterized by the equations of state (EOS) and the Bingham plastic model, which were used to describe the hydrodynamic and non-Newtonian fluid behavior, respectively. Details for the validation of the CEL technique can also be referred to our previous work (Lin *et al.* 2020). Table 1 shows the input parameters for the granular material.

Sandbox, rigid barrier, and baffle piles were defined as rigid bodies based on the Lagrangian mesh. The Eulerian mesh of 0.012 m was obtained from a series of mesh convergence studies. The results of the validation were compared to the measurement presented by Moriguchi *et al.* (2009). The results show generally good

Table 1 Input parameters for the granular material used in this study (after Lin *et al.* 2020)

	ρ (kg/m³)	EOS, U_s-U_p			Herschel-Bulkley model			
		C_0 (m/s)	S	γ	η (Pa·s)	σ_0 (Pa)	k	n
Granular material	1379	100	0	0	100	3000	4	1

Note: ρ is material density; C_0 is the bulk speed of sound; S is a linear Hugoniot slope coefficient(dU_s/dU_p); γ is Grüneisen's gamma at the reference state; U_s is the shock wave velocity; U_p is the particle velocity; η is viscosity; σ_0 is yield stress; k and n are the flow consistency and the flow behavior index in the power-law regime, respectively.

agreement between the numerical results and the measurements of the free surface configuration for the flowing granular material (see Fig. 3) and impact forces (see Table 2).

Table 2 Numerical results for the impact force exerted on a rigid barrier (after Lin *et al.* 2020)

Slope angle (°)	Peak impact force			Stable impact force		
	Experiment (N)	CEL (N)	D_{impact} (%)	Experiment (N)	CEL (N)	D_{impact} (%)
45	193.8	213.1	10.0	187.7	187.6	– 0.1
50	200.8	250.3	24.7	177.9	213.1	19.8
55	268.7	306.7	14.1	161.5	189.0	17.0
60	404.6	405.3	0.2	183.5	195.2	6.4
65	501.1	501.1	0	180.8	170.3	– 5.8

4. DESIGN OF THE CEL MODELS

The CEL models in this study mainly consist of four parts: sandbox, granular material, baffle piles, and rigid barrier (Fig. 2). The sandbox is 3.1 m in length, 1.4 m in height, and 0.3 in width. The slope angles (inclinations) considered were 45°, 55°, and 65°. The granular material, with a length of 0.5 m, a height of 0.3 m, and a width of 0.3 m, was placed on the right side of the sandbox model. The granular material flow in the sandbox under different slope angles was simulated by applying different gravity components. A rigid barrier with a length of 0.1 m, a height of 0.3 m, and a width of 0.3 m was placed in front of the granular material at a distance of 1.8 m.

Rectangular and circular baffle piles were considered in the analysis. The rectangular and circular baffle piles were set to have the same volume. Considering the size of the sandbox, the dimensions of the rectangular baffle piles were set to be 0.03 m in length, 0.03 m in width, and 0.2 m in height, and the circular baffle piles were set to be 0.01693 m in radius and 0.2 m in height.

Various positions of the baffle piles along the slope were normalized, namely the ratio of travel distance of granular material to baffle piles (L_b) and to the rigid barrier (L_r). The following values of L_b/L_r are considered: 0.01, 0.16, 0.28, 0.43, 0.58, 0.63, 0.7, and 0.73. Three layouts, named layouts A, B, and C, were designed as shown in Fig. 4. where different rows of baffle piles were installed. In this study, up to two rows of baffle piles are considered. The spacings between consecutive rows and neighboring baffles were 0.21 m and 0.07 m, respectively. The height of the baffle piles and the spacing between successive rows and neighboring rows followed Choi and Law (2015), who examined the optimal geometrical configuration of baffle piles.

The Froude number (F_r) has been identified as a key parameter for scaling the impact of granular flow on structures and can be used to achieve dynamic similarity (Hübl *et al*. 2009; Choi and Law 2015). F_r is expressed as follows:

$$F_r = \frac{v}{\sqrt{gH}} \tag{12}$$

where v is the frontal velocity before impact, g is the gravity, and H is the approach flow depth. The estimated Froude numbers of the model ranged from 1.353 to 3.809, which can be characterized as granular flows (Hübl *et al*. 2009).

The Eulerian domain was 0.05 m larger than the sandbox model in each dimension. The same Eulerian mesh of 0.012 m used in the validation was adopted for investigating the impedance effect of baffle piles on granular flow behavior. Granular material was the only object assigned to the Eulerian mesh to allow the granular media to flow through the Eulerian elements during the analysis, while the other objects, including sandbox, rigid barrier, and baffle piles were defined as rigid bodies based on the Lagrangian mesh. The input parameters for the granular material were the same as those used in the validation, as shown in Table 1.

In this study, one parameter was deviated from the baseline case to investigate the influence of the specific factors (*e.g.,* baffle pile's positions). The details of the investigated factors are listed in Table 3.

Table 3 Factors used in parametric studies

Specific factors	Values / Shapes
Baffle pile's position along the slope (m)	0.01, 0.16, 0.28, 0.43*, 0.58, 0.63, 0.7, 0.73
Slope angle (°)	45*, 55, 65
Baffle pile geometry	rectangular*, circular

* Baseline case

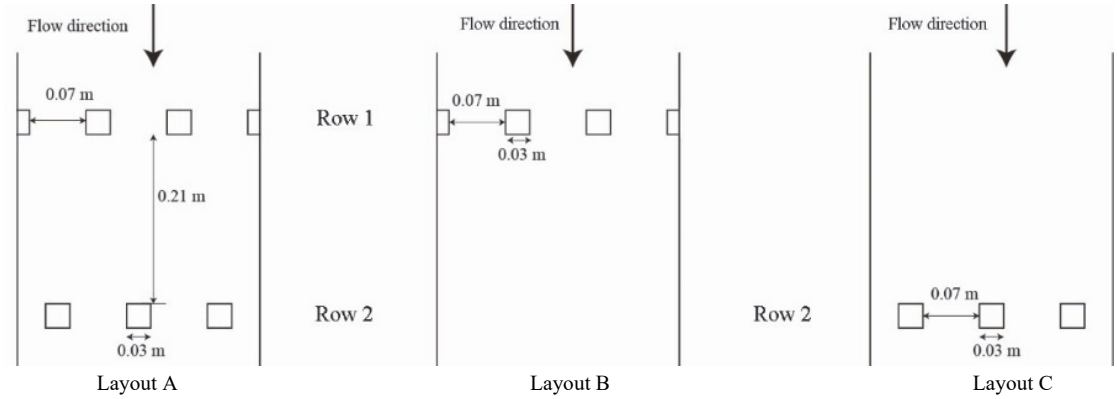

Fig. 4 Baffle piles layout and dimensions

5. RESULTS AND DISCUSSION

Figure 5 shows the observed free-surface configuration when interacting with the structures on the baseline case at different times. The granular column failed due to the static load and moved downwards. Based on the analysis, several stages can be distinguished. The granular material spread along and reached the baffle piles and impacted the first row of the baffle piles at approximately 0.53 s. On impact, three granular jets formed from the front of the granular and were discharged from space into the first row of the baffle piles. At 0.80 s, the granular jets from the center hit the second row of the baffle piles. The forward granular flow passed through the second row of the baffle piles and split into four granular jets at 1.3 s. The granular flow continued to flow downward and collided with a rigid barrier at 2.31 s. The materials gradually slowed down uniformly and settled in front of the barrier after 3.75 s. The granular flow flew the rigid barrier can also be observed in the last stage. The maximum velocity of the whole process was about 2.683 m/s.

Key findings for the impedance effect of the baffle piles on granular flow are discussed in the following sections.

5.1 Impedance Effect of Baffle Pile's Position Along the Slope

Figure 6 shows the evolution of the impact force acting on the rigid barrier at different positions of the baffle piles along the slope and without the baffle piles. As can be seen, the baffle piles can significantly reduce the impact force acting on the rigid barrier; the reduction of impact force was up to 38%. Installing the baffle piles in different positions resulted in a difference in the arrival time of granular flow to the rigid barrier. The closer the baffle piles to the downstream, the less arrival time was required for the granular flow. However, the baffle piles can help delay the arrival time, the residual acting force in the case of no baffle piles is much lower than in the case of baffle piles. Reasonably, higher velocity occurred in the case of no baffle piles, resulting in more overflow of granular materials.

The maximum impact force exerted on the rigid barrier in the various baffle pile's positions along the slope is shown in Fig. 7. The results showed that the impedance effect of the baffle pile's position along the slope can be separated into two types. When $L_b/L_r > 0.58$, the maximum impact force drastically increased. This may be because the baffle piles are so close to the rigid barrier that the impedance effect is not fully developed. The results from Fig. 6 also showed that when $L_b/L_r > 0.58$, the impact force exerted on the rigid barrier increased more rapidly. These results demonstrated that the baffle piles installation near the downstream ($L_b/L_r > 0.58$) should be avoided. A transition point in maximum impact force exerted on the rigid barrier can be found at $L_b/L_r < 0.58$. The maximum impact force exerted on the rigid barrier happened when the baffle piles were installed in the range of L_b/L_r = 0.15-0.25, while the minimum impact force exerted on the rigid barrier was observed when $L_b/L_r = 0.58$, suggesting that the installing the baffle under $L_b/L_r = 0.58$ may lead to the least impact to the downstream.

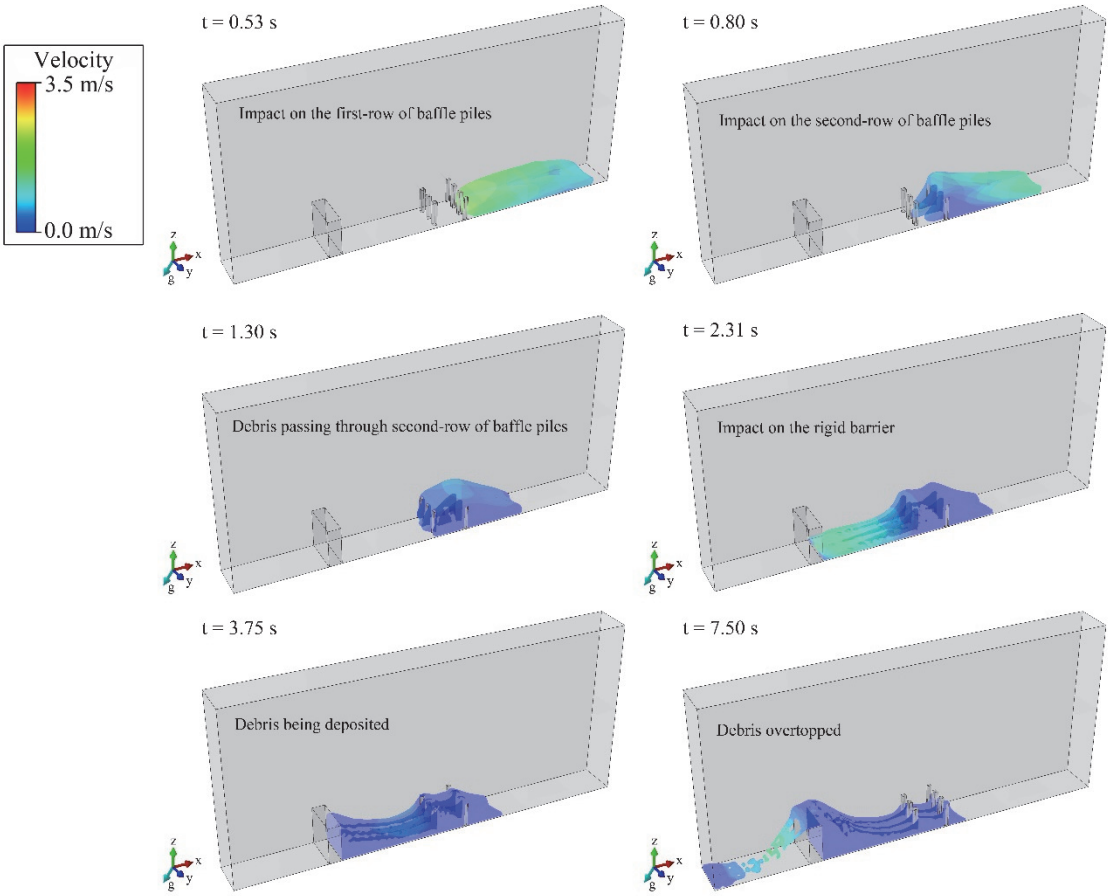

Fig. 5 The observed free-surface configuration during interaction with structures on the baseline case at different time instants

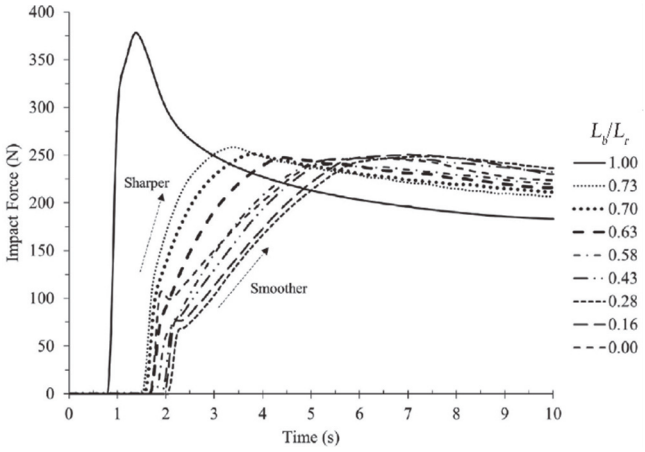

Fig. 6 The evolution of the impact force exerted on the rigid barrier in multiple baffle piles' positions and without baffle piles

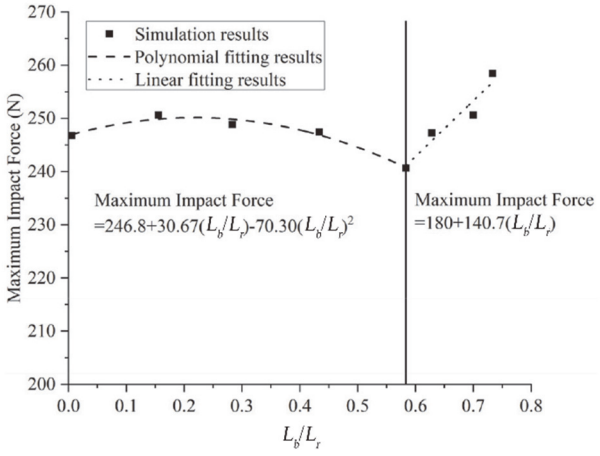

Fig. 7 The maximum impact force exerted on each baffle pile

To evaluate the destructive potential of the baffle piles installed at different positions along the slope in association with construction costs, the maximum impact force exerted on each baffle pile during the entire process is shown in Fig. 8. A similar maximum impact force of the baffle piles, regardless of the baffle pile's positions (locations), can be found, except for $L_b/L_r = 0.01$. This may be because the distance between baffle piles and granular material is too close, resulting in the velocity of the granular material hasn't been developed before impacting the baffle piles. Although a lower velocity is observed when the granular flow hits the baffle piles at a higher position, most of the granular materials hit the baffle piles simultaneously (see Fig. 9(a)), leading to a larger impact force. On the other hand, although a higher velocity was observed in the middle position when the granular flow first impacted the baffle piles, less material collided with the baffle piles, as shown in Fig. 9(b).

The impact force of different layouts (Layouts A–C) on a rigid barrier in different positions was also investigated, as shown in Fig. 10. It can be observed that using two rows of baffle piles always induces the smallest impact force and can delay the time to reach the maximum impact force compared with only using one row of baffle piles. The impact forces of layouts B and C are only slightly different from each other, except for Layout C in the downslope ($L_b/L_r > 0.58$). This difference may be caused by the fact that the baffle piles in Layout C under $L_b/L_r > 0.58$ are too close to the rigid barrier, and therefore the granular flow buried the baffle piles before hitting the rigid barrier. The results demonstrate that a minimum distance is required between the downstream and the baffle piles for the effect of the baffle piles to be fully developed.

The kinetic energy changes obtained from the CEL analyses, considering different baffle pile's positions along the slope and a case without baffle piles, were monitored and shown in Fig. 11. The kinetic energy changes in CEL are obtained by the following formulation:

$$E_K = \int_V \frac{1}{2}\rho v \cdot v \, dV \tag{13}$$

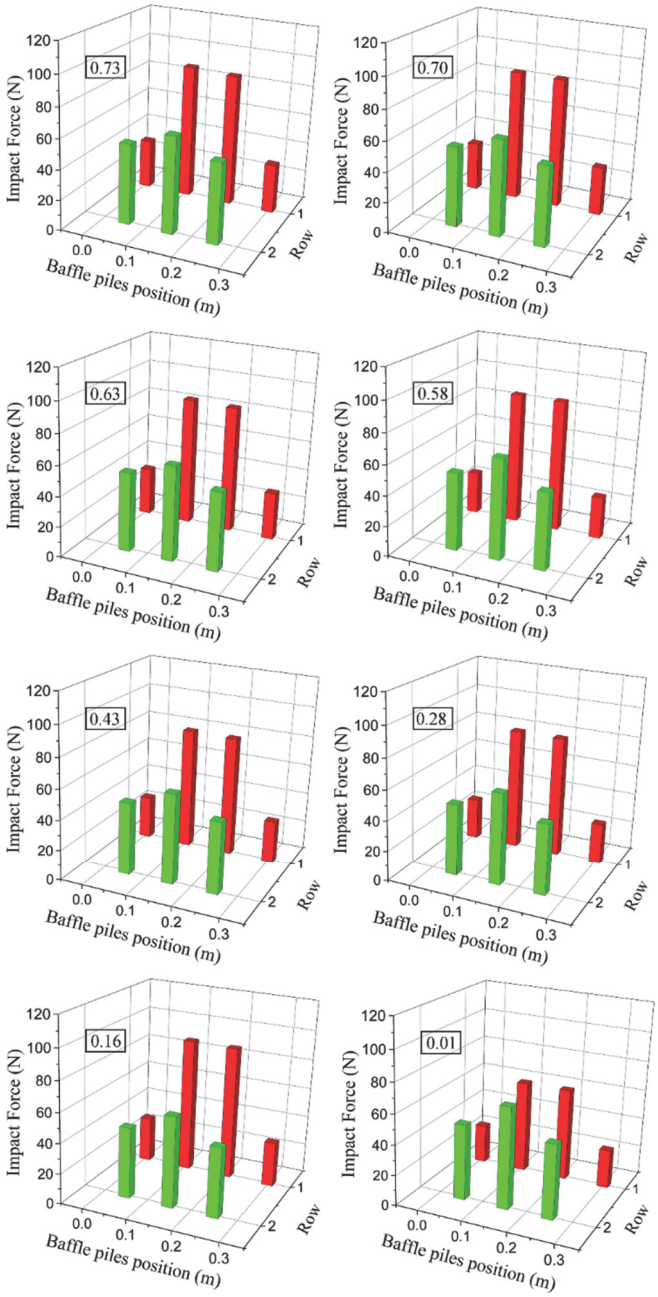

Fig. 8 The maximum impact force exerted on each baffle pile during the entire process (baffle pile's positions effects)

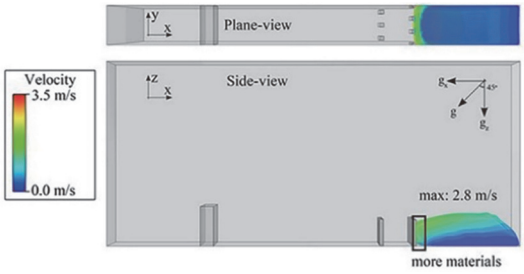

(a) $L_b/L_r = 0.16$

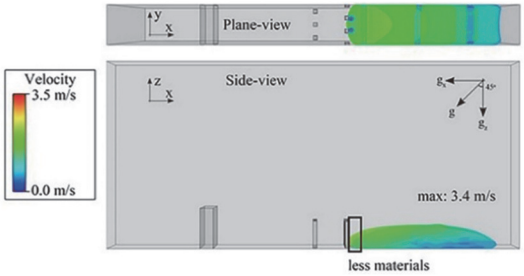

(b) $L_b/L_r = 0.43$

Fig. 9 Simulated free surface configuration

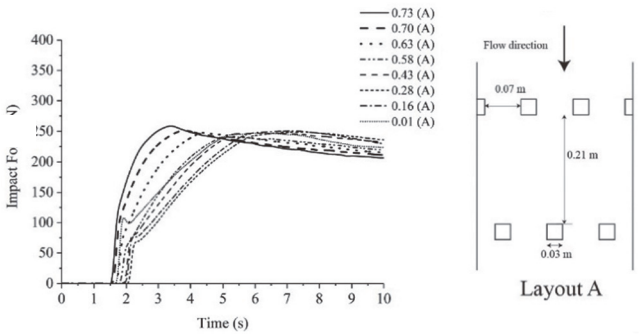

(a) Model with Layout A

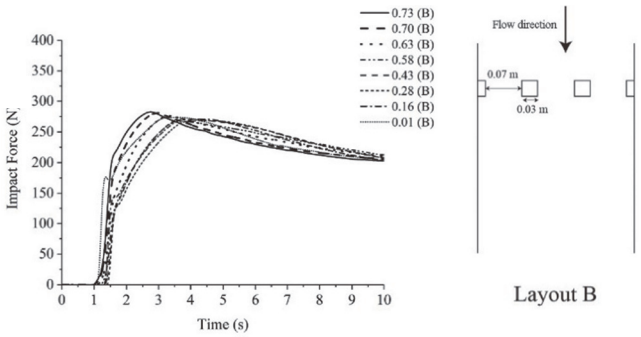

(b) Model with Layout B

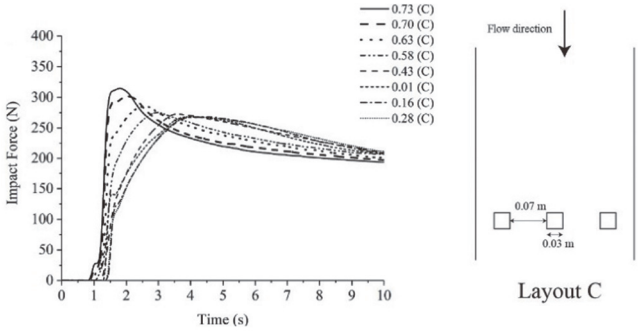

(c) Model with Layout C

Fig. 10 The impact force of rigid barrier, models with different baffle pile layouts, and installation positions

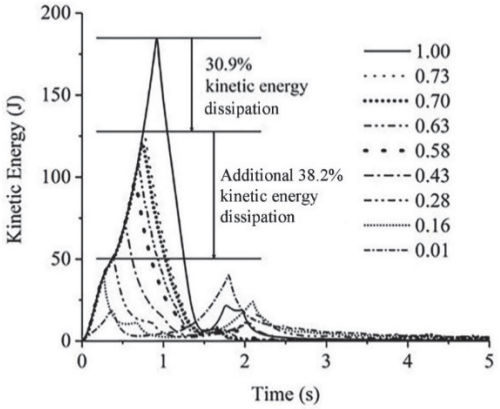

Fig. 11 T.he kinetic energy changes in different baffle pile's positions along the slope and in a case without baffle piles

where E_K is the kinetic energy, ρ is the material density, and v is the velocity vector.

When the velocity of the granular flow speeded up due to gravity, the kinetic energy increased. Then, the kinetic energy dissipated significantly when the granular flow collided with the structures. It is evident that when the baffle piles were installed upstream, namely smaller L_b/L_r, a greater dissipation would occur, resulting in lower mobility of the granular flow. This can also be explained by the fact that, with the smaller L_b/L_r, slower development of the impact on the rigid barrier would be induced. By installing the baffle piles under $L_b/L_r = 0.73$, 30.9% kinetic energy dissipation is observed. An additional 38.2% kinetic energy dissipation was observed when the baffle piles were moved from 0.73 to 0.28.

5.2 Slope Angle on Impedance Effect

Figure 12 shows the evolution of the impact force exerted on the rigid barrier at different slope angles. The results show that the baffle piles present a good impedance ability under different slope angles. The maximum impact force was drastically reduced if the baffle piles were installed. With the inclusion of baffle piles, the cases with slope angles of 45°, 55°, and 65° experienced reductions in the maximum impact force of 34.6%, 55.0%, and 28.9%, respectively. A better impedance performance was observed at steeper slope angles; however, the maximum reduction did not occur at a slope angle of 65°. This can be explained by the following phenomenon: when the slope angle was 65°, the granular flow flew and hit the rigid barrier directly after it passed the second row of the baffle piles (Fig. 13(a)). On the other hand, when the slope angle was 55°, the granular flow continued to interact with the slope after passing the second row of the baffle piles, resulting in more energy dissipation before the granular flow collided with the rigid barrier, as shown in Fig. 13(b).

To further investigate the phenomenon observed for a slope angle of 65°, the baffle piles installed under $L_b/L_r = 0.16$ with different slope angles were also analyzed. Figure 14 shows the evolution of the impact force exerted on the rigid barrier at the higher position along the slope ($L_b/L_r = 0.16$) at three different slope angles. The results indicate that installing the baffle piles can help reduce the impact force exerted on the rigid barrier, by 33.72% at 45° and 55.88% at 65°. Based on the results, to maximize the impedance effect of the baffle piles, the baffle pile should be

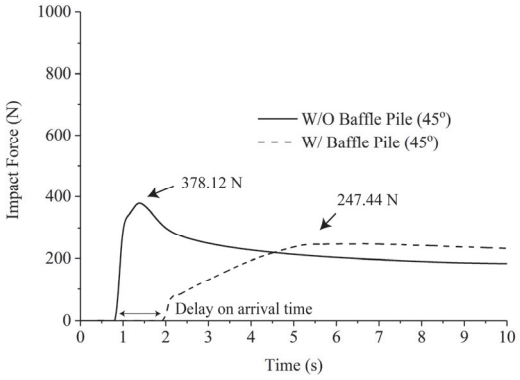

(a) Slope angle = 45°

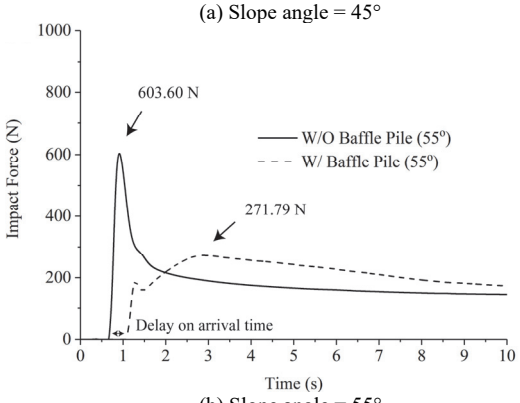

(b) Slope angle = 55°

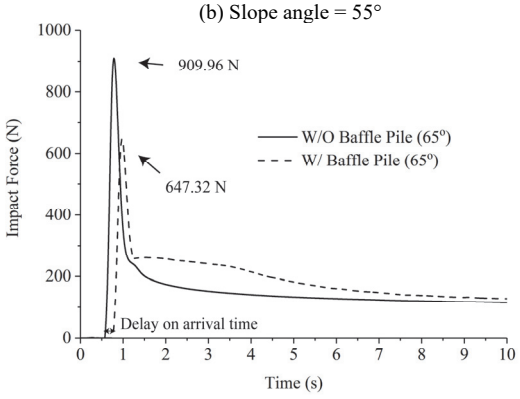

(c) Slope angle = 65°

Fig. 12 The evolution of the impact force exerted on the rigid barrier at different slope angles

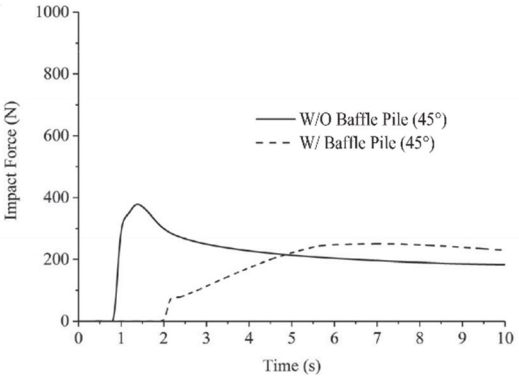

(a) Slope angle = 45°

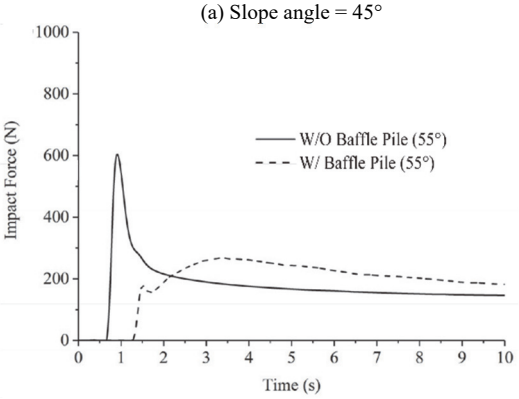

(b) Slope angle = 55°

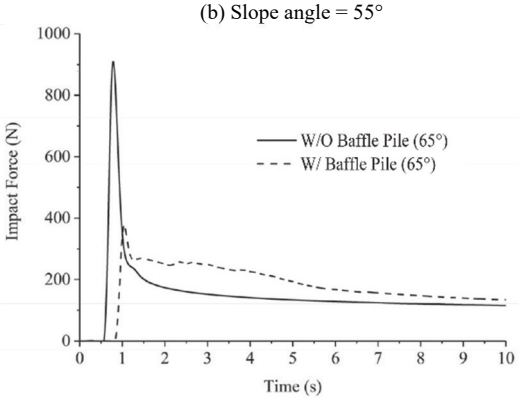

(c) Slope angle = 65°

Fig. 14 The evolution of the impact force exerted on the rigid barrier at different slope angles

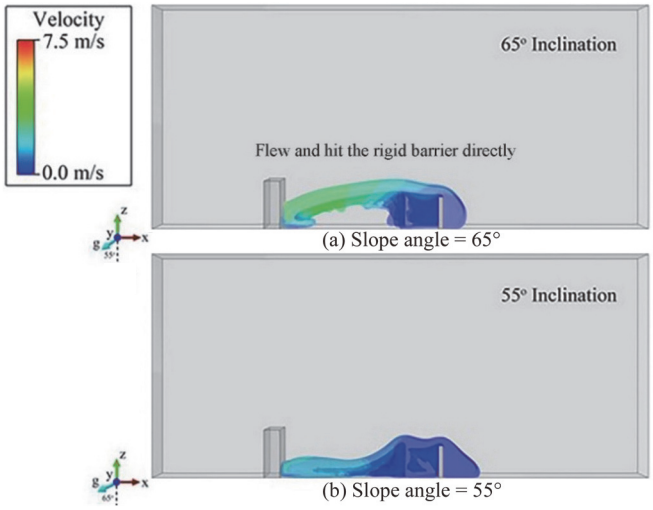

(a) Slope angle = 65°

(b) Slope angle = 55°

Fig. 13 Simulated free surface configuration

carefully considered at a steeper slope angle. Additionally, the arrival time can be delayed by installing the baffle piles; however, this effect becomes less significant if the slope angle is increased. This is because under a steeper slope angle, although the baffle piles reduced the kinetic energy, the higher mobility of the granular flows remained.

Figure 15 shows the maximum impact force acting on each baffle pile during the flow process at different slope angles. It can be seen that, overall, the maximum force acting on the baffle piles increased as the slope angle increased. Notably, the results indicate that, although a better impedance effect was found at steeper slopes, stronger baffle piles are required to prevent destruction. Note that the baffle piles were defined as rigid bodies in this study, and the failure condition of the baffle piles was not considered herein.

The kinetic energy changes in the cases with and without baffle piles under three different slope angles were also monitored and shown in Fig. 16. It can be seen that a steeper slope angle resulted in a higher maximum kinetic energy and a higher kinetic energy

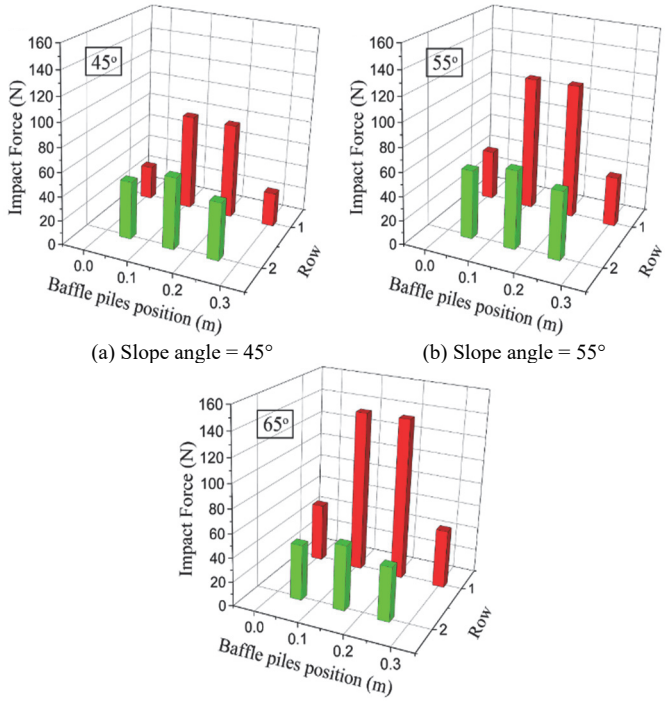

(a) Slope angle = 45° (b) Slope angle = 55°

(c) Slope angle = 65°

Fig. 15 The maximum impact force exerted on each baffle pile under different slope angles

dissipation rate. When the baffle piles were installed, significant kinetic energy dissipation was observed under various slope angles. The results indicate that the presence of the baffle piles helps to dissipate the kinetic energy, so the granular flows decelerated.

5.3 Shape of Baffle Pile on Impedance Effect

Figure 17 illustrates the evolution of the impact force exerted on the rigid barrier under the different shapes of baffle piles. Similar maximum impact force exerted on the rigid barrier and the arrival time of the granular flow to the rigid barrier were found for the circular and rectangular baffle piles.

The maximum impact force exerted on each baffle pile under different baffle pile geometries is shown in Fig. 18. It can be seen that, overall, the circular baffle piles resulted in a smaller maximum impact force being exerted on each baffle pile compared to the rectangular baffle piles. This may be due to the structural geometry, as discussed by Shen et *al*. (2018), Wang *et al*. (2018), and Huang *et al*. (2021). The structural geometry influences the kinetics of granular flows. Since the impact force was exerted on the baffle piles, the impact force can be evenly distributed to each part of the baffle piles, leading to a smaller impact force when the circular baffle piles were installed. Also, the kinetic energy dissipation showed little difference between the circular and rectangular baffle piles (Fig. 19).

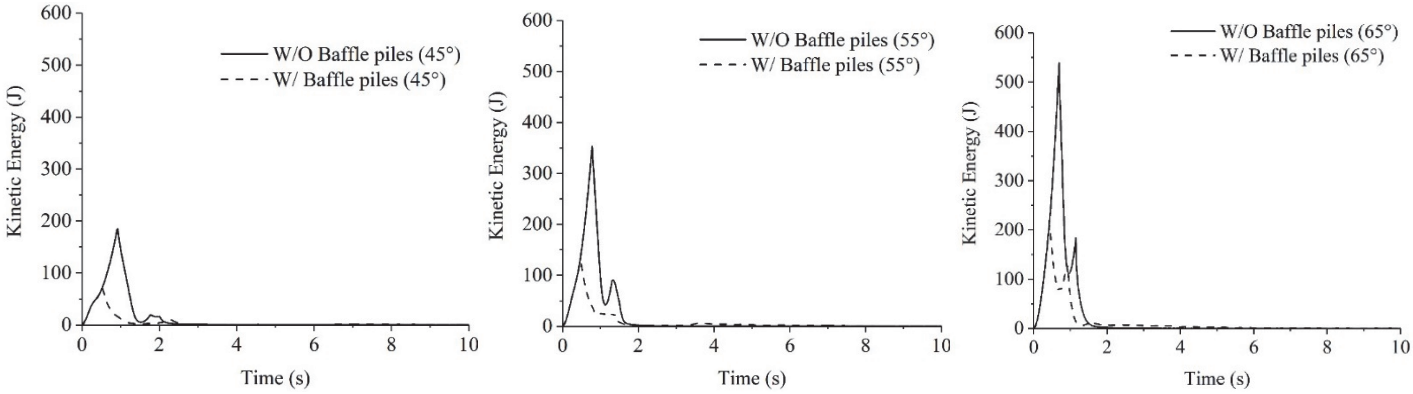

(a) Slope angle = 45° (b) Slope angle = 55° (c) Slope angle = 65°

Fig. 16 The kinetic energy changes in the cases with and without baffle piles under different slope angles

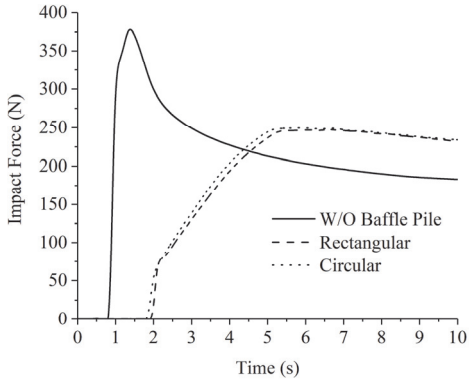

Fig. 17 The evolution of the impact force exerted on the rigid barrier under different baffle pile geometries

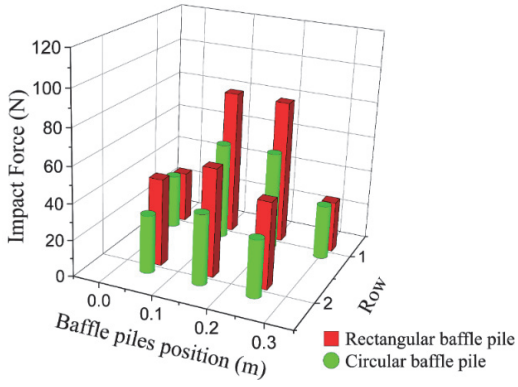

Fig. 18 The maximum impact force exerted on each baffle pile under different baffle pile geometries

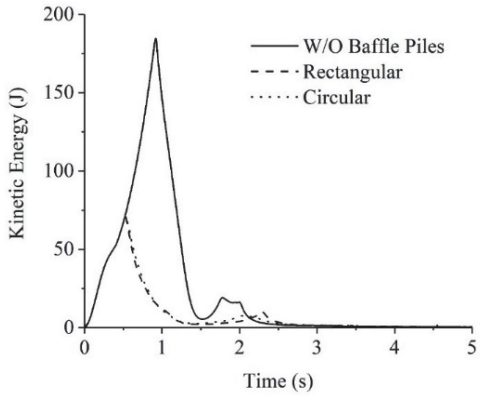

Fig. 19 The kinetic energy changes in the cases with and without baffle piles under different baffle pile geometries

6. LIMITATIONS

Some limitations of the current study are worth noting. First, the sandbox, rigid barrier, and baffle piles were defined as rigid bodies based on the Lagrangian mesh with ideal conditions. However, the rigid barriers and baffle piles may behave elastically or plastically. This may have some effect on the impact behaviors. Second, this study focused on channelized granular flows, which can be classified as one of the most hazardous landslide processes (Jakob and Weatherly 2003). The results may not be applicable to other types of granular flow. Finally, the CEL technique primarily considers mesoscale and granular flows, and collision features between particles may not be described. These limitations could be considered and discussed in future studies.

7. CONCLUSIONS

In this study, the CEL technique was used to investigate the impedance effect of baffle piles in various positions, geometries, and slope angles. This study focused on changes in the impact force acting on the rigid barrier and baffle piles, the time it takes for the granular flow to reach the rigid barrier, and the kinetic energy during the flow. Based on the results, the following conclusions can be drawn:

1. The baffle piles can significantly reduce the impact force on the rigid barrier and can delay the time for the granular flow to reach the rigid barrier.
2. Two types of impedance effects of the baffle pile's position along the slope can be bisected at a normalized distance of L_b/L_r = 0.58. Installing baffle piles beyond the normalized distance should be avoided.
3. If the baffle piles were too close to the rigid barrier, the effect of the baffle piles may not be fully realized. The smaller L_b/L_r would lead to the greater dissipation of kinetic energy.
4. Better impedance performance was observed at steeper slopes. However, stronger baffle piles are needed to prevent destruction. The flew problem should be carefully considered, especially at steeper slope angles.
5. Similar maximum impact forces exerted on the rigid barrier and the arrival time for the granular flow to reach the rigid barrier were found for circular and rectangular baffle piles. In general, the results showed that the maximum impact force for each baffle pile was lower when circular baffle piles were used.

ACKNOWLEDGMENTS

The authors thank anonymous reviewers for their constructive insight and help in improving and clarifying this manuscript.

FUNDING

The authors appreciate the support from the National Science and Technology Council, Taiwan. The research was, in part, supported by the Higher Education Sprout Project, Ministry of Education, Taiwan, Headquarters of University Advancement to the National Cheng Kung University.

DATA AVAILABILITY

The data and/or computer codes used/generated in this study are available from the corresponding author on reasonable request.

REFERENCES

Bi, Y., Du, Y., He, S., Sun, X., Wang, D., Li, X., Liang, H., and Wu, Y (2018). "Numerical analysis of effect of baffle configuration on impact force exerted from rock avalanches." *Landslides*, **15**(5), 1029-1043. https://doi.org/10.1007/s10346-018-0979-z

Bi, Y., He, S., Du, Y., Sun, X., and Li, X. (2019). "Effects of the configuration of a baffle–avalanche wall system on rock avalanches in Tibet Zhangmu: Discrete element analysis." *Bulletin of Engineering Geology and the Environment*, **78**(4), 2267-2282. https://doi.org/10.1007/s10064-018-1284-8

Chen, H. and Lee, C.F. (2004). "Geohazards of slope mass movement and its prevention in Hong Kong." *Engineering Geology*, **76**(1-2), 3-25. https://doi.org/10.1016/j.enggeo.2004.06.003

Cosenza, E., Cozzolino, L., Pianese, D., Fabbrocino, G., and Acanfora, M. (2006). "Concrete structures for mitigation of debris-flow hazard in the Montoro Inferiore Area, Southern Italy." *In 2nd International Congress, IFSC, Naples*, 1-12.

Crosta, G.B., Imposimato, S., and Roddeman, D. (2009). "Numerical modeling of 2-D granular step collapse on erodible and nonerodible surface." *Journal of Geophysical Research: Earth Surface*, 114(F3). https://doi.org/10.1029/2008JF001186

Chen, W. and Qiu, T. (2012). "Numerical simulations for large deformation of granular materials using smoothed particle hydrodynamics method." *International Journal of Geomechanics*, ASCE, **12**(2), 127-135. https://doi.org/10.1061/(ASCE)GM.1943-5622.0000149

Cui, P., Zeng, C., and Lei, Y. (2015). "Experimental analysis on the impact force of viscous debris flow." *Earth Surface Processes and Landforms*, **40**(12), 1644-1655. https://doi.org/10.1002/esp.3744

Choi, C.E. and Law, R.P. (2015). "Performance of landslide debris-resisting baffles." *HKIE Transactions*, **22**(4), 235-246. https://doi.org/10.1080/1023697X.2015.1102658

Choi, C.E., Cui, Y., Liu, L.H.D., Ng, C.W.W., and Lourenço, S.D.N. (2017). "Impact mechanisms of granular flow against

curved barriers." *Géotechnique Letters*, **7**(4), 330-338. https://doi.org/10.1680/jgele.17.00068

Coetzee, C.J. (2017). "Calibration of the discrete element method." *Powder Technology*, **310**, 104-142. https://doi.org/10.1016/j.powtec.2017.01.015

Fei, J., Jie, Y., Hong, C., and Wu, Z. (2020). "Modelling of avalanche-obstacle interaction using the depth-averaged continuum approach." *Granular Matter*, **22**(2), 1-15. https://doi.org/10.1007/s10035-020-0995-2

Hauksson, S., Pagliardi, M., Barbolini, M., and Johannesson, T. (2007). "Laboratory measurements of impact forces of supercritical granular flow against mast-like obstacles." *Cold Regions Science and Technology*, **49**(1), 54-63. https://doi.org/10.1016/j.coldregions.2007.01.007

Hübl, J., Suda, J., Proske, D., Kaitna, R., and Scheidl, C. (2009). "Debris flow impact estimation." *In Proceedings of the 11th international symposium on water management and hydraulic engineering, Ohrid, Macedonia*, **1**, 1-5. University od Ss Cyril and Methodius, Faculty of Civil Engineering, Skopje, Macedonia.

Hibbitt, Karlsson, and Sorensen. (1998). ABAQUS/Explicit: user's manual (Vol. 1). Hibbitt, Karlsson and Sorenson Incorporated.

Hsu, T.Y. (2019). "Validating and applying Coupled Eulerian-Lagrangian technique: benchmark exercise for characterizing granular flows." Master thesis, National Cheng Kung University, Tainan, Taiwan (in Chinese)

Huang, Y., Zhang, B., and Zhu, C. (2021). "Computational assessment of baffle performance against rapid granular flows." *Landslides*, **18**(1), 485-501. https://doi.org/10.1007/s10346-020-01511-6

Jakob, M. and Weatherly, H. (2003). "A hydroclimatic threshold for landslide initiation on the North Shore Mountains of Vancouver, British Columbia." *Geomorphology*, **54**(3-4), 137-156. https://doi.org/10.1016/S0169-555X(02)00339-2

Jeong, S. and Lee, K. (2019). "Analysis of the impact force of debris flows on a check dam by using a coupled Eulerian-Lagrangian (CEL) method." *Computers and Geotechnics*, **116**, 103214. https://doi.org/10.1016/j.compgeo.2019.103214

Jianbo, F., Yuxin, J., Xiaohui, S., and Xi, C. (2020). "Experimental investigation on granular flow past baffle piles and numerical simulation using a μ (I)-rheology-based approach." *Powder Technology*, **359**, 36-46. https://doi.org/10.1016/j.powtec.2019.09.069

Kasai, M., Ikeda, M., Asahina, T., and Fujisawa, K. (2009). "LiDAR-derived DEM evaluation of deep-seated landslides in a steep and rocky region of Japan." *Geomorphology*, **113**(1-2), 57-69. https://doi.org/10.1016/j.geomorph.2009.06.004

Kim, M.I., Kwak, J.H., and Kim, B.S. (2018). "Assessment of dynamic impact force of debris flow in mountain torrent based on characteristics of debris flow." *Environmental Earth Sciences*, **77**(14), 1-15. https://doi.org/10.1007/s12665-018-7707-9

Kwan, J.S., Sze, E.H., and Lam, C. (2019). "Finite element analysis for rockfall and debris flow mitigation works." *Canadian Geotechnical Journal*, **56**(9), 1225-1250. https://doi.org/10.1139/cgj-2017-062

Li, X., Yan, Q., Zhao, S., Luo, Y., Wu, Y., and Wang, D. (2020). "Investigation of influence of baffles on landslide debris mobility by 3D material point method." *Landslides*, **17**(5), 1129-1143. https://doi.org/10.1007/s10346-020-01346-1

Lee, K. and Jeong, S. (2018). "Large deformation FE analysis of a debris flow with entrainment of the soil layer." *Computers and Geotechnics*, **96**, 258-268. https://doi.org/10.1016/j.compgeo.2017.11.008

Lee, K., Kim, Y., Ko, J., and Jeong, S. (2019). "A study on the debris flow-induced impact force on check dam with-and without-entrainment." *Computers and Geotechnics*, **113**, 103104. https://doi.org/10.1016/j.compgeo.2019.103104

Li, X., Yan, Q., Zhao, S., Luo, Y., Wu, Y., and Wang, D. (2020). "Investigation of influence of baffles on landslide debris mobility by 3D material point method." *Landslides*, **17**(5), 1129-1143. https://doi.org/10.1007/s10346-020-01346-1

Lin, C.H., Hung, C., and Hsu, T.Y. (2020). "Investigations of granular material behaviors using coupled Eulerian-Lagrangian technique: From granular collapse to fluid-structure interaction." *Computers and Geotechnics*, **121**, 103485. https://doi.org/10.1016/j.compgeo.2020.103485

Luong, T.H., Baker, J.L., and Einav, I. (2020). "Spread-out and slow-down of granular flows through model forests." *Granular Matter*, **22**(1), 1-10. https://doi.org/10.1007/s10035-019-0980-9

Moriguchi, S., Borja, R.I., Yashima, A., and Sawada, K. (2009). "Estimating the impact force generated by granular flow on a rigid obstruction." *Acta Geotechnica*, **4**(1), 57-71. https://doi.org/10.1007/s11440-009-0084-5

Mast, C.M., Arduino, P., Miller, G.R., and Mackenzie-Helnwein, P. (2014). "Avalanche and landslide simulation using the material point method: flow dynamics and force interaction with structures." *Computational Geosciences*, **18**(5), 817-830. https://doi.org/10.1007/s10596-014-9428-9

Fávero Neto, A.H. and Borja, R.I. (2018). "Continuum hydrodynamics of dry granular flows employing multiplicative elastoplasticity." *Acta Geotechnica*, **13**(5), 1027-1040. https://doi.org/10.1007/s11440-018-0700-3

Ng, C.W.W., Choi, C.E., Kwan, J.S.H., Shiu, H.Y.K., Ho, K.K.S., and Koo, R.C.H. (2012). "Flume modelling of debris flow resisting baffles." *Natural Terrain Hazard Mitigation Measures*, **11**. https://repository.hkust.edu.hk/ir/Record/1783.1-56822

Ng, C.W.W., Choi, C.E., Kwan, J.S.H., Koo, R.C.H., Shiu, H.Y.K., and Ho, K.K.S. (2014). "Effects of baffle transverse blockage on landslide debris impedance." *Procedia Earth and Planetary Science*, **9**, 3-13. https://doi.org/10.1016/j.proeps.2014.06.012

Ng, C.W.W., Choi, C.E., Song, D., Kwan, J.H.S., Koo, R.C.H., Shiu, H.Y.K., and Ho, K.K.S. (2015). "Physical modeling of baffles influence on landslide debris mobility." *Landslides*, **12**(1), 1-18. https://doi.org/10.1007/s10346-014-0476-y

Nguyen, N.H., Bui, H.H., and Nguyen, G.D. (2020). "Effects of material properties on the mobility of granular flow." *Granular Matter*, **22**(3), 1-17. https://doi.org/10.1007/s10035-020-01024-y

Nguyen, T.S., Yang, K.H., Wu, Y.K., Teng, F., Chao, W.A., and Lee, W.L. (2022). Post-failure process and kinematic behavior of two landslides: Case study and material point analyses. *Computers and Geotechnics*, **148**, 104797. https://doi.org/10.1016/j.compgeo.2022.104797

Song, D., Ng, C.W.W., Choi, C.E., Zhou, G.G., Kwan, J.S., and Koo, R.C.H. (2017). "Influence of debris flow solid fraction on rigid barrier impact." *Canadian Geotechnical Journal*, **54**(10), 1421-1434. https://doi.org/10.1139/cgj-2016-0502

Shen, W., Zhao, T., Zhao, J., Dai, F., and Zhou, G.G. (2018). "Quantifying the impact of dry debris flow against a rigid barrier by DEM analyses." *Engineering Geology*, **241**, 86-96. https://doi.org/10.1016/j.enggeo.2018.05.011

Siyou, X., Lijun, S., Yuanjun, J., Xin, Q., Min, X., Xiaobo, H., and

Zhenyu, L. (2020). "Experimental investigation on the impact force of the dry granular flow against a flexible barrier." *Landslides*, **17**(6), 1465-1483. https://doi.org/10.1007/s10346-020-01368-9

Troncone, A., Conte, E., and Pugliese, L. (2019). "Analysis of the slope response to an increase in pore water pressure using the material point method." *Water*, **11**(7), 1446. https://doi.org/10.3390/w11071446

Vagnon, F. and Segalini, A. (2016). "Debris flow impact estimation on a rigid barrier." *Natural Hazards and Earth System Sciences*, **16**(7), 1691-1697. https://doi.org/10.5194/nhess-16-1691-2016

Wang, Y., Liu, X., Yao, C., Li, Y., Liu, S., and Zhang, X. (2018). "Finite release of debris flows around round and square piers." *Journal of Hydraulic Engineering*, ASCE, **144**(12), 06018015. https://doi.org/10.1061/(ASCE)HY.1943-7900.0001542

Wei, Z., Yin, G., Wang, J.G., Wan, L., and Jin, L. (2012). "Stability analysis and supporting system design of a high-steep cut soil slope on an ancient landslide during highway construction of Tehran–Chalus." *Environmental Earth Sciences*, **67**(6), 1651-1662. https://doi.org/10.1007/s12665-012-1606-2

Zhang, L., Cai, Z., Wang, L., Zhang, R., and Liu, H. (2018). "Coupled Eulerian-Lagrangian finite element method for simulating soil-tool interaction." *Biosystems Engineering*, **175**, 96-105. https://doi.org/10.1016/j.biosystemseng.2018.09.003